HHS Public Access

Author manuscript

Environ Sci Technol. Author manuscript; available in PMC 2020 January 06.

Published in final edited form as:

Environ Sci Technol. 2019 January 15; 53(2): 692–701. doi:10.1021/acs.est.8b05871.

Nitrous Oxide Is a Potent Inhibitor of Bacterial Reductive Dechlorination

Yongchao Yin[†,‡,#], **Jun Yan**[†,∥], **Gao Chen**[‡,§], **Fadime Kara Murdoch**[†,‡,#], **Nina Pfisterer**[†,‡,∇], **Frank E. Löffler**[*,†,‡,§,⊥,#]

[†]Department of Microbiology, University of Tennessee, Knoxville, Tennessee 37996, United States

[‡]Center for Environmental Biotechnology, University of Tennessee, Knoxville, Tennessee 37996, United States

[§]Department of Civil and Environmental Engineering, University of Tennessee, Knoxville, Tennessee 37996, United States

[⊥]Department of Biosystems Engineering and Soil Science, University of Tennessee, Knoxville, Tennessee 37996, United States

[∥]Key Laboratory of Pollution Ecology and Environmental Engineering, Institute of Applied Ecology, Chinese Academy of Sciences, Liaoning 110016, People's Republic of China

[#]Biosciences Division, Oak Ridge National Laboratory, Oak Ridge, Tennessee 37831, United States

Abstract

Organohalide-respiring bacteria are key players for the turnover of organohalogens. At sites impacted with chlorinated ethenes, bioremediation promotes reductive dechlorination; however, stoichiometric conversion to environmentally benign ethene is not always achieved. We demonstrate that nitrous oxide (N_2O), a compound commonly present in groundwater, inhibits organohalide respiration. N_2O concentrations in the low micromolar range decreased dechlorination rates and resulted in incomplete dechlorination of tetrachloroethene (PCE) in *Geobacter lovleyi* strain SZ and of *cis*-1,2-dichloroethene (*c*DCE) and vinyl chloride (VC) in *Dehalococcoides mccartyi* strain BAV1 axenic cultures. Presumably, N_2O interferes with reductive dechlorination by reacting with super-reduced Co(I)− corrinoids of reductive dehalogenases, which is supported by the finding that N_2O did not inhibit corrinoid-independent fumarate-to-succinate reduction in strain SZ. Kinetic analyses revealed a best fit to the noncompetitive Michaelis−Menten inhibition model and determined N_2O inhibitory constants, K_I, for PCE and

[*]**Corresponding Author:** Phone: (865) 974-4933. frank.loeffler@utk.edu.

[∇]**Present Address:** N.P.: RNA Biology and Molecular Physiology, Faculty of Biology, Bielefeld University, Bielefeld 101133, Germany.

Supporting Information

The Supporting Information is available free of charge on the ACS Publications website at DOI: 10.1021/acs.est.8b05871. Equations of inhibition models considered in kinetic analyses; raw data of initial dechlorination rates versus corresponding substrate concentrations in cell suspension assays with increasing N_2O concentrations; inhibition models tested and statistical parameters (R^2, AICc, and Sy.x values) used for ranking inhibition models; initial versus final amounts of N_2O determined in growth experiments; competitive and uncompetitive N_2O inhibition plots of PCE, *c*DCE, and VC reductive dechlorination (PDF)

The authors declare no competing financial interest.

*c*DCE dechlorination of 40.8 ± 3.8 and 21.2 ± 3.5 μM in strain SZ and strain BAV1, respectively. The lowest K_I value of 9.6 ± 0.4 μM was determined for VC to ethene reductive dechlorination in strain BAV1, suggesting that this crucial dechlorination step for achieving detoxification is most susceptible to N_2O inhibition. Groundwater N_2O concentrations exceeding 100 μM are not uncommon, especially in watersheds impacted by nitrate runoff from agricultural sources. Thus, dissolved N_2O measurements can inform about *c*DCE and VC stalls at sites impacted with chlorinated ethenes.

Graphical Abstract

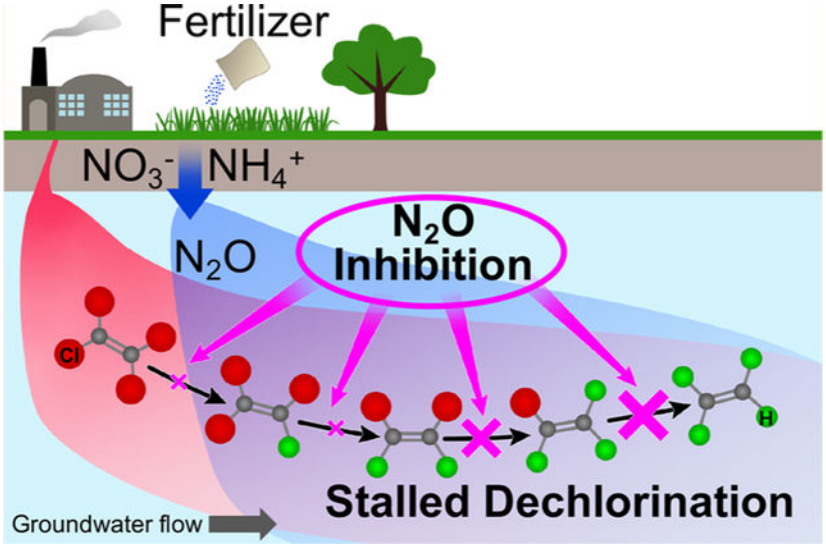

INTRODUCTION

Chlorinated solvents such as chlorinated ethenes are widespread groundwater contaminants of concern due to their adverse impact on human and ecosystem health.[1] The discovery of organohalide-respiring bacteria (OHRB) triggered the development of enhanced bioremediation treatment at sites impacted with chlorinated ethenes.[1,2] *Geobacter lovleyi* (*Geo*) strain SZ[3] reductively dechlorinates tetrachloroethene (PCE) via trichloroethene (TCE) to *cis*-1,2-dichloroethene (*c*DCE), and several strains of the species *Dehalococcoides mccartyi* (*Dhc*)[4] and *Candidatus* Dehalogenimonas etheniformans (*Dhgm*)[5] reduce *c*DCE and vinyl chloride (VC) to environmentally benign ethene. Reductive dechlorination is an electron-consuming process, and biostimulation with fermentable substrates to increase the flux of hydrogen is a commonly applied approach to enhance in situ contaminant detoxification.[2,6] Biostimulation alone or combined with bioaugmentation has been applied at many sites impacted with chlorinated ethenes, and substantial reductions in total organic chlorine are generally achieved; however, declining PCE and TCE concentrations are often associated with increasing trends in *c*DCE and VC concentrations.[7–10] Stalled reductive dechlorination may be due to a lack of electron donor (i.e., hydrogen) or unfavorable geochemical conditions such as the presence of competing electron acceptors (e.g., sulfate),[11,12] the presence of oxygen,[13] low pH conditions,[14] or the absence of organohalide-respiring Dehalococcoidia (i.e., *Dhc* and *Dhgm*).[2,15]

Interestingly, a data-mining prediction model applied to geochemical and microbial groundwater monitoring data sets collected from sites impacted with chlorinated ethenes ranked nitrate and nitrite concentrations as the most relevant predictors for in situ reductive dechlorination and detoxification potential.[16] Microcosm studies have attributed nitrate inhibition of PCE-to-*c*DCE reductive dechlorination to elevated redox potential;[7,11] however, nitrate had no inhibitory effect on PCE or TCE dechlorination in axenic cultures of *Geo* strain SZ and *Dhc* strain FL2.[3,17] These contrasting observations can be reconciled if a nitrate transformation product exerts an inhibitory effect on reductive dechlorination. Nitrous oxide (N_2O) is a known metabolite of microbial nitrogen metabolism including nitrate reduction or ammonium oxidation,[18–21] and inhibitory effects of N_2O on methanogenesis,[22–24] and in one case on PCE reductive dechlorination,[11] have been reported. Although detailed mechanistic studies are lacking, a likely explanation is the reaction of N O with cob(I)amides[25,26] and the ensuing inhibition of corrinoid-dependent enzyme systems involved in e.g., methanogenesis.[27] The reductive dehalogenase (RDase) enzyme systems catalyzing carbon−chlorine bond cleavage require a cobamide prosthetic group for function;[28–30] however, the effects of N_2O on reductive dechlorination by OHRB are largely unclear.

As global fertilizer usage continues to increase and elevated concentrations N_2O occur in groundwater,[31] detailed understanding of the impact of N_2O on relevant microbial processes, including organohalide respiration, is needed. This study explored the impact of N_2O on microbial reductive dechlorination and determined inhibitory constants (K_I values) of N_2O on reductive dechlorination of PCE in Geo strain SZ and of *c*DCE and VC in *Dhc* strain BAV1.

MATERIALS AND METHODS

Chemicals.

PCE, *c*DCE (both ≥99.5%), VC (≥99.5%), ethene (≥99.9%), Vitamin B_{12} (≥98%), sodium fumarate (≥98%), and N_2O (≥99%) were purchased from Sigma-Aldrich (St Louis, MO, USA). All other chemicals used in this study were reagent grade or of higher purity.

Bacterial Strains and Growth Conditions.

The impact of N_2O on reductive dechlorination was investigated using two organohalide-respiring isolates: *Geo* strain SZ, a corrinoid-prototroph capable of dechlorinating PCE and TCE to *c*DCE,[3,32] and *Dhc* strain BAV1, a corrinoid-auxotroph capable of dechlorinating cDCE and VC to nontoxic ethene.[4,33] Both cultures were grown in 160 mL serum bottles containing a CO_2/N_2 (20/80, vol/vol) headspace and 100 mL of synthetic, bicarbonate-buffered (30 mM, pH 7.3) and reduced (0.2 mM Na_2S and 0.2 mM L-cysteine) mineral salt medium as described.[30,34] Strain SZ cultures received 5 mM acetate as electron donor, 0.28 mM PCE (38 μmol/bottle), 10 mM fumarate, or both PCE and fumarate as electron acceptors, and a vitamin B_{12}-free Wolin vitamin solution.[35] *Dhc* strain BAV1 culture vessels received 10 mL of hydrogen, 0.8 mM (90 μmol/bottle) *c*DCE or 0.25 mM (40 μmol/bottle) VC, and 5 mM acetate as electron donor, electron acceptor, and carbon source, respectively. *Dhc* strain BAV1 culture vessels received the Wolin vitamin stock solution containing

vitamin B_{12} to achieve a final concentration of 25 μg L^{-1}. For inoculation, culture vessels received 3% (v/v) inocula from actively dechlorinating cultures maintained under the same conditions. All experiments used triplicate culture vessels, and culture bottles without N_2O and without inoculum served as positive and negative controls, respectively. Culture vessels were incubated without agitation at 30 °C in the dark with the stoppers facing up.

Inhibition Experiments.

For *Geo* strain SZ cultures, undiluted N_2O gas was directly added to incubation vessels using plastic syringes (BD, Franklin Lakes, NJ, USA) to achieve final aqueous N_2O concentrations of 9.5, 19.1, and 57.3 μM in PCE-amended cultures, of 191.4 μM and 10 mM in fumarate-amended cultures, and of 191.4 μM in cultures grown with both PCE and fumarate. For *Dhc* strain BAV1 cultures, undiluted or 10-fold-diluted (with N_2) N_2O gas was added with plastic syringes to achieve final aqueous phase N_2O concentrations of 9.5, 19.1, and 57.3 μM in *c*DCE-amended vessels and of 2.9, 5.7, and 19.1 μM in VC-amended vessels. The aqueous phase concentrations (in μM) of N_2O in all medium bottles were calculated from the headspace concentrations using a dimensionless Henry's constant of 1.94 for N_2O at 30 °C[36] according to $C_{aq} = C_g/H_{cc}$, where C_{aq}, C_g, and H_{cc} are the aqueous concentration (in μM), the headspace concentration (in μmol L^{-1}), and the dimensionless Henry's constant, respectively. Average dechlorination rates were calculated based on the continuous accumulation of dechlorination products (i.e., before stable product concentrations were observed). Since each reductive dechlorination step is associated with the release of one chloride ion (Cl^-), the average dechlorination rates determined in growth experiments are reported as the total amount of Cl^- released per volume per unit time (i.e., μmol Cl^- L^{-1} d^{-1}).

Whole Cell Suspension Dechlorination Assays.

Biomass for whole cell suspension assays was harvested by centrifugation at 10 000*g* at 4 °C for 30 min from 1.6 L *Geo* strain SZ and *Dhc* strain BAV1 cultures that had dechlorinated three feedings of PCE and *c*DCE, respectively. Inside an anoxic chamber (Coy Laboratory Products Inc., MI, USA), the supernatants were decanted, and the pellets were suspended in 8−10 mL of reduced mineral salts medium. For protein quantification, triplicate 0.2 (strain SZ) and 1.0 mL (strain BAV1) of concentrated cell suspensions were transferred to 2 mL screw cap tubes containing 20 mg of 0.1 mm diameter glass beads, and cells were broken at room temperature using a Bead Ruptor (OMNI, GA, USA) at a speed of 6.0 m s^{-1} for three 10 min cycles with 2 min breaks. After centrifugation at 13 000*g* for 2 min to remove cell debris, protein content in the supernatants was estimated using the Bradford assay[37] on a plate reader (BioTek Instruments, VT, USA). To ensure consistency between replicate experiments, cell suspensions of both isolates were freshly prepared following identical procedures.

Dechlorination assays for rate determinations were performed in 8 mL glass vials sealed with Teflon-lined butyl rubber septa held in place with aluminum crimps. Each vial contained 3.80−4.86 mL of reduced mineral salts medium with 5 mM acetate, a N_2/CO_2 (80/20, vol/vol) headspace for *Geo* strain SZ, and a H_2/CO_2 (80/20, vol/vol) headspace for *Dhc* strain BAV1. Electron donor was provided in at least 40-fold excess of the theoretical

demand to ensure that reductive dechlorination was not electron-donor limited. For *Geo* strain SZ cell suspensions, 36−1100 μL of an aqueous 1 mM PCE stock solution was added directly to the assay vials to achieve final aqueous PCE concentrations ranging from 5 to 150 μM. For *Dhc* strain BAV1 cell suspensions, 2−550 μL of *c*DCE stock (from a 5.0 mM aqueous stock solution) or 12−630 μL of VC stock (from a 2.0 mM aqueous stock solution) was added to achieve final aqueous *c*DCE and VC concentrations ranging from 1 to 500 μM and 3 to 150 μM, respectively. The total aqueous volume in all vials was 4.9 mL before introducing 0.1 mL of cell suspension. Replicate vials at each initial PCE and *c*DCE concentration received N_2O to achieve 0, 10, and 60 μM, and VC-amended vials received N_2O to achieve 0, 15, and 50 μM dissolved phase N_2O concentrations. The added N_2O concentrations were quantified in all assay vials prior to and at the end of the incubation period and determined constant N_2O concentrations. Following equilibration, each assay vial received 0.1 mL of the respective cell suspension (corresponding to 56.3 ± 2.2 μg of protein per vial for *Geo* strain SZ and 19.7 ± 1.4 μg of protein per vial for *Dhc* strain BAV1) using plastic syringes to start dechlorination activity. Vials that received 0.1 mL of sterile mineral salt medium instead of cell suspension and vials that received 0.1 mL of heat-killed cell suspension served as negative controls. During the 6 h assay incubation, liquid samples (1 mL) were collected from sacrificial assay vials every 60 min and transferred to 20 mL glass autosampler vials containing 0.1 mL of 25 mM H_2SO_4 to terminate dechlorination activity. The cell titers and substrate concentrations were chosen such that the dechlorination rates could be determined within the 6 h incubation period and no more than 80% of the initial chlorinated ethene concentration had been consumed at the end of the incubation period.

Analytical Procedures.

Chlorinated ethenes and ethene were analyzed with an Agilent G1888 headspace sampler connected to an Agilent 7890 gas chromatograph (GC) equipped with a flame ionization detector (method detection limit ≈ 0.2 μM) and a DB-624 capillary column (60 m length × 0.32 mm diameter, 1.8 μm film thickness).[34] Fumarate and succinate were quantified using an Agilent 1200 series high-performance liquid chromatography system equipped with an Aminex HPX-87H column and a dual-wavelength absorbance detector set to 210 nm.[38] N_2O was analyzed by injecting 100 μL headspace samples into an Agilent 7890A GC equipped with an HP-PLOT Q column (30 m length × 0.320 mm diameter, 20 μm film thickness) and a microelectron capture detector. The OD measurements were conducted with a PerkinElmer Lambda 35 UV−vis spectrophotometer by transferring 1 mL cell suspension into a cuvette and recording readings at 600 nm.

Dechlorination Kinetics and Inhibition Models.

The shortest doubling times reported for *Geo* strain SZ and *Dhc* strain BAV1 are 6 h[3] and 2.2 days,[4,33] respectively. Therefore, additional cell growth was considered negligible over the assay period (<6 h) and confirmed by constant OD_{600} values. For this reason, the Michaelis−Menten model (Table S1), rather than the Monod model for systems involving cell growth, was used to analyze the cell suspension dechlorination data. Therefore, the half-velocity constant K_m, rather than the Monod half-saturation constant K_s, was applied in the analyses of cell suspension kinetic parameters. For each treatment at a different initial substrate concentration [S], an initial dechlorination rate v, normalized to the amount of

protein per vial, in units of nmol Cl^- released min^{-1} mg $protein^{-1}$, was calculated from the sum of all dechlorination products measured with the GC. In brief, the amended PCE, *c*DCE, or VC concentrations in the respective assay vials served as the initial substrate concentrations, and the corresponding dechlorination rates were determined from the slope of progression curves representing total Cl^- released. The linear regression analysis included five data points and at least three for the assays with a low initial chlorinated ethene concentration. Thus, each datum point in the Michaelis− Menten plots represents a dechlorination rate extracted from one initial substrate concentration (Tables S2−S4).

The maximum dechlorination rate V_{max} and the half-velocity constant K_m for each treatment were calculated using the Michaelis−Menten nonlinear regression method in the Enzyme Kinetics Module for SigmaPlot 13 (Systat Software Inc., Chicago, IL, USA). This software module evaluated competitive, noncompetitive, and uncompetitive inhibition models for best fit to the rate data based on the highest coefficient of determination (R^2), the lowest corrected Akaike's Information Criterion (AICc) values, and the lowest standard deviation of the residuals (Sy.x.). The best-fit model (i.e., noncompetitive inhibition) was used to determine the inhibitory constant, K_I, for N_2O on reductive dechlorination. For data visualization, Michaelis−Menten (V over [S]), Lineweaver−Burk ($1/V$ over 1/[S]), and Dixon ($1/V$ over [I]) plots were generated using the SigmaPlot Enzyme Kinetics Module for each inhibition model and the different electron acceptors (i.e., PCE, *c*DCE, and VC).

RESULTS

N_2O Affects Reductive Dechlorination Performance in *Geobacter lovleyi* Strain SZ Cultures.

In the absence of N_2O, *Geo* strain SZ cultures completely dechlorinated 38.1 ± 3.1 μmol of PCE to stoichiometric amounts of *c*DCE over a 5 day incubation period, and an average PCE-to-*c*DCE dechlorination rate of 155.6 ± 27.2 μmol Cl^- L^{-1} d^{-1} was measured (Figure 1A). Cultures amended with 9.5 μM or higher concentrations of N_2O exhibited decreased dechlorination rates and incomplete PCE-to-*c*DCE dechlorination. In the presence of 9.5 μM N_2O, *Geo* strain SZ cultures dechlorinated the initial amount of PCE (38.0 ± 3.9 μmol) at a rate of 90.0 ± 21.6 μmol Cl^- L^{-1} d^{-1}, leading to an extended time period of at least 7 days to achieve complete consumption of PCE. Although PCE was completely consumed in cultures that received 9.5 μM N_2O, small amounts of TCE (7.6 ± 0.3 μmol) remained, even after an extended incubation period of 180 days (data not shown). With the addition of 19.1 μM N_2O, the average PCE dechlorination rate in *Geo* strain SZ cultures decreased to 64.2 ± 4.6 μmol Cl^- L^{-1} d^{-1}, and no more than 78 ± 3.4% of the initial amount of PCE (38.5 ± 1.1 μmol) was dechlorinated. Following an extended incubation period of 180 days, PCE (9.9 ± 0.2 μmol), TCE (6.6 ± 1.6 μmol), and *c*DCE (25.0 ± 3.2 μmol) were measured in strain SZ cultures that had received an initial dose of 38.5 ± 1.1 μmol of PCE and 19.1 μM N_2O. A further decline in dechlorination rate to 12.0 ± 2.1 μmol Cl^- L^{-1} d^{-1} was observed in cultures that received 57.3 μM N_2O, and 63.4 ± 4.5% of the initial amount of PCE (38.3 ± 3.7 μmol) remained in culture bottles at the termination of the experiments (Figure 1A). In all culture bottles with observed inhibition of dechlorination activity, electron donor (i.e., 5 mM acetate) was not limiting electron-acceptor reduction. Furthermore, consistent with the

absence of N_2O reductase (nos) operons in the genome of Geo strain SZ,[32] the amended N_2O remained constant throughout the experiment.

In addition to catalyzing PCE-to-*c*DCE dechlorination, *Geo* strain SZ also derives energy from acetate oxidation coupled to fumarate to succinate reduction.[3] In contrast to organohalide respiration catalyzed by corrinoid-dependent reductive dehalogenases, fumarate respiration via fumarate reductase does not involve a corrinoid-dependent enzyme system.[39] Therefore, investigating the impact of N_2O on fumarate reduction by *Geo* strain SZ cultures served as a control experiment to illustrate the selective effect of N_2O on the PCE RDase in *Geo* strain SZ. As shown in Figure 1B, the presence of 191.4 μM and 10 mM N_2O did not impact fumarate to succinate reduction rates and extents in Geo strain SZ cultures. In the absence of N_2O, Geo strain SZ reduced PCE and fumarate concomitantly (Figure 1C, top); however, in cultures amended with 191.4 μM N_2O, only fumarate was reduced to succinate and no PCE reductive dechlorination occurred (Figure 1C, bottom).

N_2O Affects *c*DCE and VC Reductive Dechlorination Performance in Dhc strain BAV1 Cultures.

Without N_2O, *Dhc* strain BAV1 dechlorinated *c*DCE (97.2 ± 3.1 μmol) to stoichiometric amounts of ethene (102.3 ± 6.1 μmol) within a 14-day incubation period at an average *c*DCE-to-ethene dechlorination rate of 146.1 ± 21.6 μmol Cl^- L^{-1} d^{-1} (Figure 2A). In contrast, cultures amended with 9.5 μM or higher N_2O concentrations all exhibited incomplete transformation of *c*DCE and VC and required longer incubation periods (up to 28 days) before stable dechlorination product patterns were observed. Cultures that received 9.5 μM N_2O showed a significantly lower dechlorination rate of 66.8 ± 21.6 μmol Cl^- L^{-1} d^{-1}, and the initial amount of *c*DCE (97.2 ± 1.2 μmol) was dechlorinated to a mixture of VC (74.1 ± 1.2 μmol) and ethene (23.1 ± 0.7 μmol). Cultures that received 29.0 μM N_2O dechlorinated only about one-half (50.7 ± 3.3%) of the initial amount of *c*DCE (96.3 ± 1.1 μmol) to predominantly VC (48.8 ± 3.2 μmol) at a rate of 24.4 ± 1.1 μmol Cl^- L^{-1} d^{-1}, and only small amounts of ethene (4.7 ± 0.2%) were produced. At a higher N_2O concentration of 57.3 μM, strain BAV1 dechlorinated *c*DCE to VC at a dechlorination rate of 18.9 ± 0.7 μmol Cl^- L^{-1} d^{-1}, no ethene was formed, and about one-third (26.3 ± 0.4 μmol) of the initial amount of *c*DCE remained. Extended incubation periods of up to 6 months did not result in further dechlorination in all tested strain BAV1 culture vessels with N_2O. Notably, in all N_2O-amended Dhc strain BAV1 cultures, the VC-to-ethene dechlorination step occurred at such low rates resulting in VC rather than ethene formation as the major product.

To further investigate the impact of N_2O on the reductive dechlorination of VC, *Dhc* strain BAV1 cultures amended with VC as electron acceptor received N_2O at concentrations of 2.9, 5.7, and 19.1 μM. Cultures without N_2O completely dechlorinated the initial amount of 41.2 ± 0.4 μmol of VC to ethene within 11 days at an average VC dechlorination rate of 37.2 ± 2.7 μmol Cl^- L^{-1} d^{-1} (Figure 2B). N_2O had a profound impact on VC dechlorination in *Dhc* strain BAV1 cultures, and the VC dechlorination rates decreased to 18.3 ± 2.1 and 9.8 ± 0.4 μmol Cl^- L^{-1} d^{-1} in the presence of 2.9 and 5.7 μM N_2O, respectively. Compared to the complete VC to ethene conversion in control incubations without N_2O, the amount of VC dechlorinated to ethene was diminished by 37.0 ± 1.3% and 76.2 ± 4.1%, respectively,

in cultures amended with 2.9 and 5.7 μM N_2O. The most pronounced inhibition was observed in *Dhc* strain BAV1 cultures that received 19.1 μM of N_2O (Figure 2B), and only negligible amounts (<1.6 ± 0.6 μmol) of ethene were formed even after extended incubation periods of 180 days, indicating that the VC to ethene step was particularly susceptible to N_2O inhibition.

Quantification of N_2O Inhibition in Whole Cell Suspension Dechlorination Assays.

To further investigate the inhibitory effects of N_2O on reductive dechlorination, whole cell suspension assays were performed. Plots of dechlorination rates versus initial substrate concentrations with increasing N_2O concentrations are presented in Figures 3 and 4. In all cases, the maximum dechlorination rates decreased with the addition of increasing N_2O concentrations. In *Geo* strain SZ cell suspensions without N_2O addition, a maximum PCE-to-*c*DCE dechlorination rate ($V_{max,PCE}$) of 76.3 ± 2.6 nmol Cl^- released min^{-1} mg $protein^{-1}$ was calculated using nonlinear regression in the Michaelis−Menten model (Figure 3A and Table 1). With the addition of 10 and 60 μM N_2O, $V_{max,PCE}$ in *Geo* strain SZ cell suspensions declined to 61.3 ± 4.1 and 30.9 ± 4.2 nmol Cl^- released min^{-1} mg $protein^{-1}$, respectively. Even more pronounced inhibitory effects of N_2O were observed for *c*DCE and VC dechlorination in *Dhc* strain BAV1 assays. In the presence of 10 and 60 μM N_2O, the maximum *c*DCE-to-VC dechlorination rate decreased from a $V_{max,cDCE}$ of 119.4 ± 2.1 nmol Cl^- released min^{-1} mg $protein^{-1}$ in assays without N_2O to 81.1 ± 5.1 and 31.2 ± 2.4 nmol Cl^- released min^{-1} mg $protein^{-1}$, respectively (Figure 4A and Table 1). The strongest inhibitory effect of N_2O was observed in whole cell suspension assays of strain BAV1 with VC as electron acceptor. Compared to the maximum VC-to-ethene dechlorination rate $V_{max,VC}$ of 123.3 ± 2.2 nmol Cl^- released min^{-1} mg $protein^{-1}$ without N_2O, the addition of 15 and 50 μM N_2O reduced $V_{max,VC}$ to 78.9 ± 2.1 and 19.9 ± 1.3 nmol Cl^- released min^{-1} mg $protein^{-1}$, respectively (Figure 4C and Table 1). No dechlorination was detected in control incubations (data not shown), confirming that suspended cells, rather than any abiotic reactions, were responsible for the observed dechlorination activity.

Kinetic Parameters Reveal Pronounced N_2O Inhibition.

The experimental data generated in *Geo* strain SZ cell suspension assays (Table S2) fit the Michaelis−Menten model and the corresponding Lineweaver−Burk plot ($R^2 > 0.95$) (Figure 3, Figure S1). A maximum PCE dechlorination rate $V_{max,PCE}$ of 76.3 ± 2.6 nmol Cl^- released min^{-1} mg $protein^{-1}$ and a half-velocity constant $K_{m,PCE}$ of 25.1 ± 2.9 μM characterized PCE-to-*c*DCE dechlorination kinetics for strain SZ in the absence of N_2O (Table 1, Figure 3B). Without N_2O and in the presence of 10 and 60 μM N_2O, the PCE-to-*c*DCE dechlorination data fit the competitive, uncompetitive, and noncompetitive inhibition models ($R^2 > 0.90$); however, the noncompetitive inhibition model exhibited the highest R^2 and the lowest AICc and Sy.x. values (Figure 3 and Table S5). Using the noncompetitive inhibition model, an inhibitory constant, K_I, of N_2O for PCE dechlorination in *Geo* strain SZ whole cell suspensions of 40.8 ± 3.8 μM was determined (inserted Dixon plot, Figure 3B; Table 1).

The experimental data generated in *Dhc* strain BAV1 whole cell suspension assays (Tables S3 and S4) also fit the Michaelis− Menten model simulations and the corresponding

Lineweaver− Burk plots (R^2 > 0.90) (Figure 4, Figures S2 and S3). In the presence of increasing N_2O concentrations, both *c*DCE-to-VC and VC-to-ethene reductive dechlorination data showed the best fit to the noncompetitive inhibition model based on the highest R^2 and the lowest AICc and Sy.x. values (Figure 4 and Table S5). While *Dhc* strain BAV1 assays produced comparable $V_{max,cDCE}$ and $V_{max,VC}$ values of 119.4 ± 2.1 and 123.3 ± 2.2 nmol Cl^- released min^{-1} mg $protein^{-1}$, respectively, the K_I of N_2O for *c*DCE dechlorination (21.2 ± 3.5 μM) was approximately 2-fold greater than that for VC dechlorination (9.6 ± 0.4 μM) (inserted Dixon plots, Figures 4B and 4D; Table 1), consistent with the greater inhibitory effect of N_2O observed for the VC dechlorination step. To investigate if the differences in susceptibility of the *c*DCE and VC dechlorination steps to N_2O resulted from different affinities of the BvcA RDase for *c*DCE and VC, the K_m values for these two electron acceptors were compared. On the basis of the *Dhc* strain BAV1 assays, similar $K_{m,cDCE}$ (19.9 ± 2.5 μM) and $K_{m,VC}$ (18.9 ± 1.3 μM) values were determined (Figure 4B and 4D; Table 1), indicating that the substrate affinity of the BvcA RDase does not explain the more potent inhibition of the VC-to-ethene dechlorination step by N_2O.

DISCUSSION

Effects of N_2O on Corrinoid-Dependent Processes.

Toxic effects of N_2O were first observed in the mid-1950s after two patients died following prolonged N_2O inhalation.[40] This incident triggered studies to elucidate the mechanism underlying N_2O toxicity, and detailed investigations revealed that N_2O reacts with cobalt-containing corrinoids (e.g., cobalamin) when the coordinated cobalt atom is in the reduced Co(I) state.[25,26] Due to the vital roles of enzyme systems with corrinoid prosthetic groups,[30,41] the N_2O-mediated oxidation of the Co(I) supernucleophile interferes with key metabolic functions in all domains of life.[42,43] For example, N_2O inhibits the corrinoid-dependent methionine synthase (MetH) required for the biosynthesis of the essential amino acid methionine.[44] When used as inhalation anesthetic for human patients, N_2O can lead to a malfunction of MetH, resulting in elevated levels of homocysteine in plasma (i.e., hyperhomocysteinemia).[45] Patients generally recover from N_2O exposure after 3−4 days,[44] presumably through de novo MetH synthesis or replenishment of Co(I) corrinoid.[46]

The lowest reported N_2O concentration that affected MetH activity in animals and humans was around 4.1 mM (~1000 ppm);[46] however, much lower N_2O concentrations inhibited members of the Bacteria and Archaea, presumably due to the more diverse roles of corrinoid-dependent enzyme systems in their metabolisms.[41] For example, in the denitrifying bacterium Paracoccus denitrificans strain PD1222, 0.1 mM N_2O not only repressed MetH but also modulated the expression of anabolic genes under the control of vitamin B_{12} riboswitches.[47] To compensate for the loss of MetH function, organisms such as *P. denitrificans* and *Escherichia coli* activate a corrinoid-independent methionine synthase, MetE.[41,47] Geo strain SZ possesses both the metE and the metH genes,[32] which may explain the observation that up to 10 mM N_2O did not inhibit the bacterium's growth with fumarate in defined minimal medium. In contrast, N_2O at micromolar concentrations inhibited the growth of *Geo* strain SZ cultures when PCE served as the sole electron acceptor. These observations corroborate that the inhibitory effect of N_2O to organisms varies markedly

based on whether corrinoid-dependent enzyme systems are essential for key metabolic steps, including respiratory energy conservation.

OHRB as a Model To Study the Effects of N_2O Inhibition.

A key feature of OHRB is the involvement of corrinoid-dependent RDases in electron transfer to the chlorinated organohalogen electron acceptor.[1,28,29,48] Functional and structural analyses demonstrated that RDases represent a distinct subfamily of corrinoid-dependent enzymes, and a Co(I) supernucleophile is crucial for RDases to initiate the cleavage of carbon−chlorine bonds.[28,29,49] Since corrinoid-dependent RDases are essential in the energy metabolism of OHRB, N_2O inhibition on Co(I) corrinoid-dependent RDases can be readily observed by quantitative measurement of dechlorination activity and growth when alternate electron acceptors are absent or the energy metabolism of the OHRB is restricted to chlorinated electron acceptors, as is the case for *Dhc*.[4] This effect was convincingly demonstrated in both *Geo* strain SZ and *Dhc* strain BAV1 cultures amended with chlorinated electron acceptors and N_2O. Thus, OHRB are excellent model organisms to assess the inhibitory effects of N_2O on enzymes involving the Co(I) supernucleophile in catalysis. Consistent with this assumption, experimental results showed that N_2O at micromolar concentrations exhibited strong inhibitory effects on reductive dechlorination performance in both *Geo* strain SZ and *Dhc* strain BAV1 cultures. Theoretically, a shortage of methionine caused by N_2O inhibition on MetH could also have affected dechlorination activity; however, growth of *Geo* strain SZ with fumarate was not impaired at much higher N_2O concentrations of up to 10 mM, indicating that N_2O inhibition of RDases diminished dechlorination performance.

The PCE-to-*c*DCE dechlorinating *Geo* strain SZ tolerated at least 3-fold higher N_2O concentrations than *Dhc* strain BAV1 before cessation of dechlorination activity was observed, which possibly relates to strain SZ's ability for de novo cobamide biosynthesis.[32] Active cobamide biosynthesis may allow strain SZ to maintain some level of catalytically active PCE RDase. In contrast, the characterized obligate organohalide-respiring *Dhc* strains[4,50] and *Dehalogenimonas* spp., including the VC-respiring *Candidatus* Dehalogenimonas etheniformans,[5] cannot de novo synthesize corrinoid, although exceptions may exist.[51] All characterized cDCE and VC dechlorinators strictly require exogenous corrinoid, which renders these bacteria more susceptible to N_2O inhibition, and low micromolar concentrations of N_2O (i.e., 3−10 μM) repressed the growth of the corrinoid-auxotroph Dhc strain BAV1. Unlike corrinoid-auxotrophic Dehalococcoidia, the majority of PCE-to-TCE- and TCE-to-*c*DCE-dechlorinating OHRB are corrinoid prototrophs,[52] a feature that may enable these organisms to tolerate higher N_2O concentrations. The difference in the ability for de novo corrinoid biosynthesis is one possible explanation why PCE and TCE dechlorination to *c*DCE is generally achieved at sites with nitrate,[16,53] but ethene is not produced.[7–10]

Corrinoid-dependent enzyme systems fulfill essential metabolic functions for organisms in all branches of life, but only a subset of the bacteria and the archaea have the machinery for de novo corrinoid biosynthesis.[41,54,55] Therefore, N_2O effects on microbial processes that

hinge on the activity of corrinoid-dependent enzyme systems may expand beyond organohalide respiration.

Elevated Groundwater N_2O and Kinetic Parameters.

Based the current day atmospheric N_2O concentration of 330 ppb, the theoretical equilibrium concentration of N_2O in groundwater should be around 7 nM, assuming no mass transfer limitations; however, much higher groundwater N_2O concentrations were reported, indicating other sources exist.[31,56] For example, the increased usage of synthetic nitrogen fertilizer for agricultural production causes substantial nitrate runoff and elevated N_2O concentrations in groundwater.[19,31] Indeed, correlations between fertilizer application and associated nitrate runoff with elevated groundwater N_2O concentrations have been established.[19,56] Nitrate is not conservative, and processes including denitrification,[18,19] respiratory ammonification (i.e., dissimilatory nitrate reduction to ammonium, DNRA)[57] and ensuing nitrification,[21] as well as chemodenitrification[38] contribute to the formation of N_2O. Such biogeochemical processes are likely responsible for elevated N_2O concentrations, and up to 140 μM N_2O was observed in watersheds impacted by agricultural activities.[31] Thus, the N_2O concentrations measured in many groundwater aquifers exceed the theoretical equilibrium with atmospheric N_2O by up to 5 orders in magnitude, and intensified agriculture will exacerbate this issue.

A K_I value indicates the inhibitor (i.e., N_2O) concentration at which the maximum reaction rate V_{max} (i.e., the reductive dechlorination rates of chlorinated ethenes) is reduced by 50%. The determined K_I values for N_2O on reductive dechlorination of PCE, *c*DCE, and VC are in the range of 40, 20, and 10 μM, respectively, well below reported N_2O concentrations encountered in many groundwater aquifers, particularly at sites impacted by agricultural runoff.[31] Consequently, N_2O inhibition could be a major cause for incomplete reductive dechlorination and *c*DCE and VC stalls observed at field sites.[7–10,53] Of note, a 50% $V_{max,cDCE}$ and $V_{max,VC}$ inhibition occurred in strain BAV1 at 2- and 4-fold lower N_2O concentrations, respectively, compared to the same level of inhibition of $V_{max,PCE}$ in strain SZ. The higher K_I values for N_2O determined for *Geo* strain SZ compared to strain BAV1 may be related to the ability of strain SZ for de novo corrinoid biosynthesis (see above) or to mechanistic differences in the dechlorination steps catalyzed by the PceA versus the BvcA RDases. Similar K_m values for *c*DCE and VC were determined in strain BAV1, indicating the organism exhibits similar affinities for *c*DCE and VC; however, the 2-fold higher K_I value for the *c*DCE versus the VC dechlorination step cannot be easily explained considering the same BvcA RDase is involved in both dechlorination steps,[52,58] and detailed mechanistic studies are warranted.

Predicting the fate of chlorinated ethenes at bioremediation sites relies on accurate estimates of the intrinsic kinetic parameters of OHRB;[59] however, kinetic constants determinations using various dechlorinating cultures at different cell densities reported highly variable V_{max} and K_m values (or K_S values when Monod kinetics were applied).[12,60,61] Likely explanations for these discrepancies are that different, potentially competing types of dechlorinators with distinct RDases and present in varied abundances contributed to reductive dechlorination.[12,62,63] The current study accomplished kinetic measurements in

axenic cultures under defined conditions and over short incubation periods (<6 h, no growth occurred), which facilitates the determination of intrinsic kinetic parameters.[59] The Michaelis−Menten model simulations predicted the behaviors of *Geo* strain SZ and *Dhc* strain BAV1 ($R^2 > 0.90$), and both organisms fit the noncompetitive inhibition model ($R^2 > 0.96$) with micromolar levels of N_2O as the inhibitor. These findings imply N_2O as a noncompetitive inhibitor that oxidizes the Co(I) corrinoid cofactor of RDases, thereby decreasing reductive dechlorination rates.

Implications for in Situ Bioremediation.

Electron donor (i.e., hydrogen) limitations,[6] nutrient availability (e.g., fixed nitrogen),[15] unfavorable redox potential,[7,11] low pH conditions,[14] or toxic and/or inhibitory effects of cocontaminants (e.g., sulfide, chloroform, 1,1,1-trichloroethane)[12,62] can impact the microbial reductive dechlorination process. The findings of the current study indicate that decreased reductive dechlorination performance can be the result of N_2O inhibition. A common strategy to improve in situ degradation of chlorinated ethenes involves the injection of nutrients (i.e., biostimulation), typically fermentable substrates aimed at increasing the flux of hydrogen.[2,64] The formulations can include fertilizer (nitrate, ammonium, urea, phosphorus) to proactively address possible nutrient limitations.[2,13,15,65] Biogeochemical transformations of fixed nitrogen will generate N O[21,38,57] and exert inhibitory effects on microbial reductive dechlorination, which can result in undesirable *c*DCE or VC stalls. Thus, practitioners should carefully evaluate the need for fixed nitrogen additions to avoid possible N_2O inhibition.

The inhibitory constants, K_I, for N_2O inhibition of PCE, *c*DCE, and VC dechlorination were within the N_2O concentration ranges observed in groundwater aquifers (i.e., up to 143 μM),[31] suggesting that N_2O should be of concern at contaminated sites where practitioners seek to rely on microbial reductive dechlorination as a remedial strategy. Considering the relevance of the microbial reductive dechlorination process for achieving cleanup goals and the commonality of elevated N_2O concentrations in aquifers, groundwater monitoring regimes should include nitrate/nitrite and N_2O measurements, so that potential inhibition and *c*DCE and VC stalls can be explained and predicted.

Supplementary Material

Refer to Web version on PubMed Central for supplementary material.

ACKNOWLEDGMENTS

This work was supported by the Strategic Environmental Research and Development Program (SERDP project ER-2312) and, in part, by awards from the National Institute of Environmental Health Sciences (R01ES024294) and the National Science Foundation (Dimensions DEB1831599). Y.Y participates in the China-University of Tennessee One-Hundred Scholars Program, and the authors acknowledge the support by the China Scholarship Council and the University of Tennessee.

REFERENCES

(1). Adrian L; Löffler FE Organohalide-respiring bacteria; Springer: Berlin, Heidelberg, 2016.

(2). Löffler FE; Edwards EA Harnessing microbial activities for environmental cleanup. Curr. Opin. Biotechnol 2006, 17 (3), 274–284. [PubMed: 16697178]

(3). Sung Y; Fletcher KE; Ritalahti KM; Apkarian RP; Ramos-Hernandez N; Sanford RA; Mesbah NM; Löffler FE *Geobacter lovleyi* sp. nov. strain SZ, a novel metal-reducing and tetrachloroethene-dechlorinating bacterium. Appl. Environ. Microbiol 2006, 72 (4), 2775–2782. [PubMed: 16597982]

(4). Löffler FE; Yan J; Ritalahti KM; Adrian L; Edwards EA; Konstantinidis KT; Müller JA; Fullerton H; Zinder SH; Spormann AM *Dehalococcoides mccartyi gen. nov., sp. nov.*, obligately organohalide-respiring anaerobic bacteria relevant to halogen cycling and bioremediation, belong to a novel bacterial class, *Dehalococcoidia classis nov.*, order *Dehalococcoidales ord. nov.* and family *Dehalococcoidaceae fam. nov.*, within the phylum *Chloroflexi*. Int. J. Syst. Evol. Microbiol 2013, 63 (2), 625–635. [PubMed: 22544797]

(5). Yang Y; Higgins SA; Yan J; Simsir B; Chourey K; Iyer R; Hettich RL; Baldwin B; Ogles DM; Löffler FE Grape pomace compost harbors organohalide-respiring Dehalogenimonas species with novel reductive dehalogenase genes. ISME J 2017, 11 (12), 2767–2780. [PubMed: 28809851]

(6). Fennell DE; Gossett JM; Zinder SH Comparison of butyric acid, ethanol, lactic acid, and propionic acid as hydrogen donors for the reductive dechlorination of tetrachloroethene. Environ. Sci. Technol 1997, 31 (3), 918–926.

(7). Schmidt KR; Tiehm A Natural attenuation of chloroethenes: identification of sequential reductive/oxidative biodegradation by microcosm studies. Water Sci. Technol 2008, 58 (5), 1137–1145. [PubMed: 18824815]

(8). Amaral HI; Aeppli C; Kipfer R; Berg M Assessing the transformation of chlorinated ethenes in aquifers with limited potential for natural attenuation: added values of compound-specific carbon isotope analysis and groundwater dating. Chemosphere 2011, 85 (5), 774–781. [PubMed: 21741066]

(9). Dugat-Bony E; Biderre-Petit C; Jaziri F; David MM; Denonfoux J; Lyon DY; Richard JY; Curvers C; Boucher D; Vogel TM; Peyretaillade E; Peyret P *In situ* TCE degradation mediated by complex dehalorespiring communities during biostimulation processes. Microb. Biotechnol 2012, 5 (5), 642–653. [PubMed: 22432919]

(10). Tillotson JM; Borden RC Rate and extent of chlorinated ethene removal at 37 ERD sites. J. Environ. Eng 2017, 143 (8), 04017028.

(11). Nelson DK; Hozalski RM; Clapp LW; Semmens MJ; Novak PJ Effect of nitrate and sulfate on dechlorination by a mixed hydrogen-fed culture. Biorem. J 2002, 6 (3), 225–236.

(12). Berggren DR; Marshall IP; Azizian MF; Spormann AM; Semprini L Effects of sulfate reduction on the bacterial community and kinetic parameters of a dechlorinating culture under chemostat growth conditions. Environ. Sci. Technol 2013, 47 (4), 1879–1886. [PubMed: 23316874]

(13). Steffan RJ; Schaefer CE Current and future bioremediation applications: bioremediation from a practical and regulatory perspective In Organohalide-respiring bacteria; Adrian L, Löffler FE, Eds.; Springer Berlin Heidelberg: Berlin, Heidelberg, 2016; pp 517–540.

(14). Yang Y; Capiro NL; Marcet TF; Yan J; Pennell KD; Löffler FE Organohalide respiration with chlorinated ethenes under low pH conditions. Environ. Sci. Technol 2017, 51 (15), 8579–8588. [PubMed: 28665587]

(15). Lendvay JM; Löffler FE; Dollhopf M; Aiello MR; Daniels G; Fathepure BZ; Gebhard M; Heine R; Helton R; Shi J Bioreactive barriers: a comparison of bioaugmentation and biostimulation for chlorinated solvent remediation. Environ. Sci. Technol 2003, 37 (7), 1422–1431.

(16). Lee J; Im J; Kim U; Löffler FE A data mining approach to predict In situ detoxification potential of chlorinated ethenes. Environ. Sci. Technol 2016, 50 (10), 5181–5188. [PubMed: 27116079]

(17). He J; Sung Y; Krajmalnik-Brown R; Ritalahti KM; Löffler FE Isolation and characterization of *Dehalococcoides sp.* strain FL2, a trichloroethene (TCE)-and 1,2-dichloroethene-respiring anaerobe. Environ. Microbiol 2005, 7 (9), 1442–1450. [PubMed: 16104866]

(18). Zumft WG Cell biology and molecular basis of denitrification. Microbiol Mol. Biol. Rev 1997, 61 (4), 533–616. [PubMed: 9409151]

(19). Thomson AJ; Giannopoulos G; Pretty J; Baggs EM; Richardson DJ Biological sources and sinks of nitrous oxide and strategies to mitigate emissions. Philos. Trans. R. Soc., B 2012, 367 (1593), 1157–1168.

(20). Zhu X; Burger M; Doane TA; Horwath WR Ammonia oxidation pathways and nitrifier denitrification are significant sources of N_2O and NO under low oxygen availability. Proc. Natl. Acad. Sci. U. S. A 2013, 110 (16), 6328–6333. [PubMed: 23576736]

(21). Daims H; Lücker S; Wagner M A new perspective on microbes formerly known as nitrite-oxidizing bacteria. Trends Microbiol. 2016, 24 (9), 699–712. [PubMed: 27283264]

(22). Balderston WL; Payne WJ Inhibition of methanogenesis in salt marsh sediments and whole-cell suspensions of methanogenic bacteria by nitrogen oxides. Appl. Environ. Microbiol 1976, 32 (2), 264–269. [PubMed: 970945]

(23). Klüber HD; Conrad R Inhibitory effects of nitrate, nitrite, NO and N_2O on methanogenesis by *methanosarcina barkeri* and *Methanobacterium bryantii*. FEMS Microbiol. Ecol 1998, 25, 331–339.

(24). Tugtas AE; Pavlostathis SG Inhibitory effects of nitrogen oxides on a mixed methanogenic culture. Biotechnol. Bioeng 2007, 96 (3), 444–455. [PubMed: 16865733]

(25). Banks RGS; Henderson RJ; Pratt JM Reactions of gases in solution. Part III. Some reactions of nitrous oxide with transition-metal complexes. J. Chem. Soc. A 1968, No. 0, 2886–2889.

(26). Blackburn R; Kyaw M; Swallow AJ Reaction of cob(I)alamin with nitrous oxide and cob(III)alamin. J. Chem. Soc., Faraday Trans. 1 1977, 73 (0), 250–255.

(27). Fischer R; Thauer RK Methanogenesis from acetate in cell extracts of *Methanosarcina barkeri*: isotope exchange between CO_2 and the carbonyl group of acetyl-CoA, and the role of H_2. Arch. Microbiol 1990, 153 (2), 156–162.

(28). Bommer M; Kunze C; Fesseler J; Schubert T; Diekert G; Dobbek H Structural basis for organohalide respiration. Science 2014, 346 (6208), 455–458. [PubMed: 25278505]

(29). Payne KA; Quezada CP; Fisher K; Dunstan MS; Collins FA; Sjuts H; Levy C; Hay S; Rigby SE; Leys D Reductive dehalogenase structure suggests a mechanism for B_{12}-dependent dehalogenation. Nature 2015, 517 (7535), 513–516. [PubMed: 25327251]

(30). Yan J; Bi M; Bourdon AK; Farmer AT; Wang PH; Molenda O; Quaile AT; Jiang N; Yang Y; Yin Y; Şimşir B; Campagna SR; Edwards EA; Löffler FE Purinyl-cobamide is a native prosthetic group of reductive dehalogenases. Nat. Chem. Biol 2017, 14 (1), 8–14. [PubMed: 29106396]

(31). Jurado A; Borges AV; Brouyere S Dynamics and emissions of N_2O in groundwater: A review. Sci. Total Environ 2017, 584–585, 207–218.

(32). Wagner DD; Hug LA; Hatt JK; Spitzmiller MR; Padilla-Crespo E; Ritalahti KM; Edwards EA; Konstantinidis KT; Löffler FE Genomic determinants of organohalide-respiration in *Geobacter lovleyi*, an unusual member of the *Geobacteraceae*. BMC Genomics 2012, 13 (1), 200. [PubMed: 22616984]

(33). He J; Ritalahti KM; Yang KL; Koenigsberg SS; Löffler FE Detoxification of vinyl chloride to ethene coupled to growth of an anaerobic bacterium. Nature 2003, 424 (6944), 62–65. [PubMed: 12840758]

(34). Yan J; Şimşir B; Farmer AT; Bi M; Yang Y; Campagna SR; Löffler FE The corrinoid cofactor of reductive dehalogenases affects dechlorination rates and extents in organohalide-respiring *Dehalococcoides mccartyi*. ISME J. 2016, 10 (5), 1092–1101. [PubMed: 26555247]

(35). Wolin EA; Wolin MJ; Wolfe RS Formation of methane by bacterial extracts. J. Biol. Chem 1963, 238 (8), 2882–2886. [PubMed: 14063318]

(36). Sander R Compilation of Henry's law constants (version 4.0) for water as solvent. Atmos. Chem. Phys 2015, 15 (8), 4399–4981.

(37). Bradford MM A rapid and sensitive method for the quantitation of microgram quantities of protein utilizing the principle of protein-dye binding. Anal. Biochem 1976, 72 (1), 248–254. [PubMed: 942051]

(38). Onley JR; Ahsan S; Sanford RA; Löffler FE Denitrification by *Anaeromyxobacter dehalogenans*, a common soil bacterium lacking the nitrite reductase genes *nirS and nirK*. Appl. Environ. Microbiol 2018, 84 (4), e01985–17. [PubMed: 29196287]

(39). Iverson TM; Luna-Chavez C; Cecchini G; Rees DC Structure of the *Escherichia coli* fumarate reductase respiratory complex. Science 1999, 284 (5422), 1961–1966. [PubMed: 10373108]

(40). Lassen HCA; Henriksen E; Neukirch F; Kristensen H Treatment of tetanus. Severe bone-marrow depression after prolonged nitrous-oxide anaesthesia. Lancet 1956, 267, 527–530.

(41). Matthews RG Cobalamin- and corrinoid-dependent enzymes. Met Ions Life Sci. 2009, 6, 53–114. [PubMed: 20877792]

(42). Drummond JT; Matthews RG Nitrous oxide degradation by cobalamin-dependent methionine synthase: characterization of the reactants and products in the inactivation reaction. Biochemistry 1994, 33, 3732–3741. [PubMed: 8142373]

(43). Drummond JT; Matthews RG Nitrous oxide inactivation of cobalamin-dependent methionine synthase from *Escherichia coli*: characterization of the damage to the enzyme and prosthetic group. Biochemistry 1994, 33 (12), 3742–3750. [PubMed: 8142374]

(44). Royston BD; Nunn JF; Weinbren HK; Royston D; Cormack RS Rate of inactivation of human and rodent hepatic methionine synthase by nitrous oxide. Anesthesiology 1988, 68 (2), 213–216. [PubMed: 3341574]

(45). Singer MA; Lazaridis C; Nations SP; Wolfe GI Reversible nitrous oxide-induced myeloneuropathy with pernicious anemia: case report and literature review. Muscle Nerve 2008, 37 (1), 125–129. [PubMed: 17623854]

(46). Weimann J Toxicity of nitrous oxide. Bailliere's Best Pract. Res., Clin. Anaesthesiol 2003, 17 (1), 47–61.

(47). Sullivan MJ; Gates AJ; Appia-Ayme C; Rowley G; Richardson DJ Copper control of bacterial nitrous oxide emission and its impact on vitamin B_{12}-dependent metabolism. Proc. Natl. Acad. Sci. U. S. A 2013, 110 (49), 19926–19931. [PubMed: 24248380]

(48). Wang S; Qiu L; Liu X; Xu G; Siegert M; Lu Q; Juneau P; Yu L; Liang D; He Z; Qiu R Electron transport chains in organohalide-respiring bacteria and bioremediation implications. Biotechnol. Adv 2018, 36 (4), 1194–1206. [PubMed: 29631017]

(49). Fincker M; Spormann AM Biochemistry of catabolic reductive dehalogenation. Annu. Rev. Biochem 2017, 86, 357–386. [PubMed: 28654328]

(50). Seshadri R; Adrian L; Fouts DE; Eisen JA; Phillippy AM; Methe BA; Ward NL; Nelson WC; Deboy RT; Khouri HM; Kolonay JF; Dodson RJ; Daugherty SC; Brinkac LM; Sullivan SA; Madupu R; Nelson KE; Kang KH; Impraim M; Tran K; Robinson JM; Forberger HA; Fraser CM; Zinder SH; Heidelberg JF Genome sequence of the PCE-dechlorinating bacterium *Dehalococcoides ethenogenes*. Science 2005, 307 (5706), 105–108. [PubMed: 15637277]

(51). Brisson VL; West KA; Lee PKH; Tringe SG; Brodie EL; Alvarez-Cohen L Metagenomic analysis of a stable trichloroethene-degrading microbial community. ISME J. 2012, 6 (9), 1702–1714. [PubMed: 22378537]

(52). Schubert T; Adrian L; Sawers RG; Diekert G Organohalide respiratory chains: composition, topology and key enzymes. FEMS Microbiol Ecol 2018, 94 (4), fiy035.

(53). Verce MF; Madrid VM; Gregory SD; Demir Z; Singleton MJ; Salazar EP; Jackson PJ; Halden RU; Verce A A long-term field study of *in situ* bioremediation in a fractured conglomerate trichloroethene source zone. Biorem. J 2015, 19 (1), 18–31.

(54). Shelton AN; Seth EC; Mok KC; Han AW; Jackson SN; Haft DR; Taga ME Uneven distribution of cobamide biosynthesis and dependence in bacteria predicted by comparative genomics. ISME J. 2018, DOI: 10.1038/s41396-018-0304-9.

(55). Zhang Y; Rodionov DA; Gelfand MS; Gladyshev VN Comparative genomic analyses of nickel, cobalt and vitamin B_{12} utilization. BMC Genomics 2009, 10 (1), 78. [PubMed: 19208259]

(56). Reay DS; Davidson EA; Smith KA; Smith P; Melillo JM; Dentener F; Crutzen PJ Global agriculture and nitrous oxide emissions. Nat. Clim. Change 2012, 2 (6), 410–416.

(57). Yoon S; Cruz-García C; Sanford R; Ritalahti KM; Löffler FE Denitrification versus respiratory ammonification: environmental controls of two competing dissimilatory NO_3^-/NO_2^- reduction pathways *in Shewanella loihica* strain PV-4. ISME J. 2015, 9 (5), 1093–1104. [PubMed: 25350157]

(58). Tang S; Chan WWM; Fletcher KE; Seifert J; Liang X; Löffler FE; Edwards EA; Adrian L Functional characterization of reductive dehalogenases by using blue native polyacrylamide gel electrophoresis. Appl. Environ. Microbiol 2013, 79 (3), 974–981. [PubMed: 23204411]

(59). Huang D; Becker JG Determination of intrinsic monod kinetic parameters for two heterotrophic tetrachloroethene (PCE)-respiring strains and insight into their application. Biotechnol. Bioeng 2009, 104 (2), 301–311. [PubMed: 19593756]

(60). Baelum J; Scheutz C; Chambon JC; Jensen CM; Brochmann RP; Dennis P; Laier T; Broholm MM; Bjerg PL; Binning PJ; Jacobsen CS The impact of bioaugmentation on dechlorination kinetics and on microbial dechlorinating communities in subsurface clay till. Environ. Pollut 2014, 186, 149–157. [PubMed: 24374375]

(61). Mayer-Blackwell K; Fincker M; Molenda O; Callahan B; Sewell H; Holmes S; Edwards EA; Spormann AM 1,2-dichloroethane exposure alters the population structure, metabolism, and kinetics of a trichloroethene-dechlorinating *Dehalococcoides mccartyi* consortium. Environ. Sci. Technol 2016, 50 (22), 12187–12196. [PubMed: 27809491]

(62). Chan WW; Grostern A; Löffler FE; Edwards EA Quantifying the effects of 1,1,1-trichloroethane and 1,1-dichloroethane on chlorinated ethene reductive dehalogenases. Environ. Sci. Technol 2011, 45 (22), 9693–9702. [PubMed: 21955221]

(63). Buttet GF; Murray AM; Goris T; Burion M; Jin B; Rolle M; Holliger C; Maillard J Coexistence of two distinct *Sulfurospirillum* populations respiring tetrachloroethene - genomic and kinetic considerations. FEMS Microbiol Ecol 2018, 94 (5), fiy018.

(64). McCarty PL Groundwater contamination by chlorinated solvents: History, remediation technologies and strategies In In Situ remediation of chlorinated solvent plumes; Stroo HF, Ward CH, Eds.; Springer New York: New York, 2010; pp 1–28.

(65). Schaefer CE; Lippincott DR; Steffan RJ Field-scale evaluation of bioaugmentation dosage for treating chlorinated ethenes. Groundwater Monit. Rem 2010, 30 (3), 113–124.

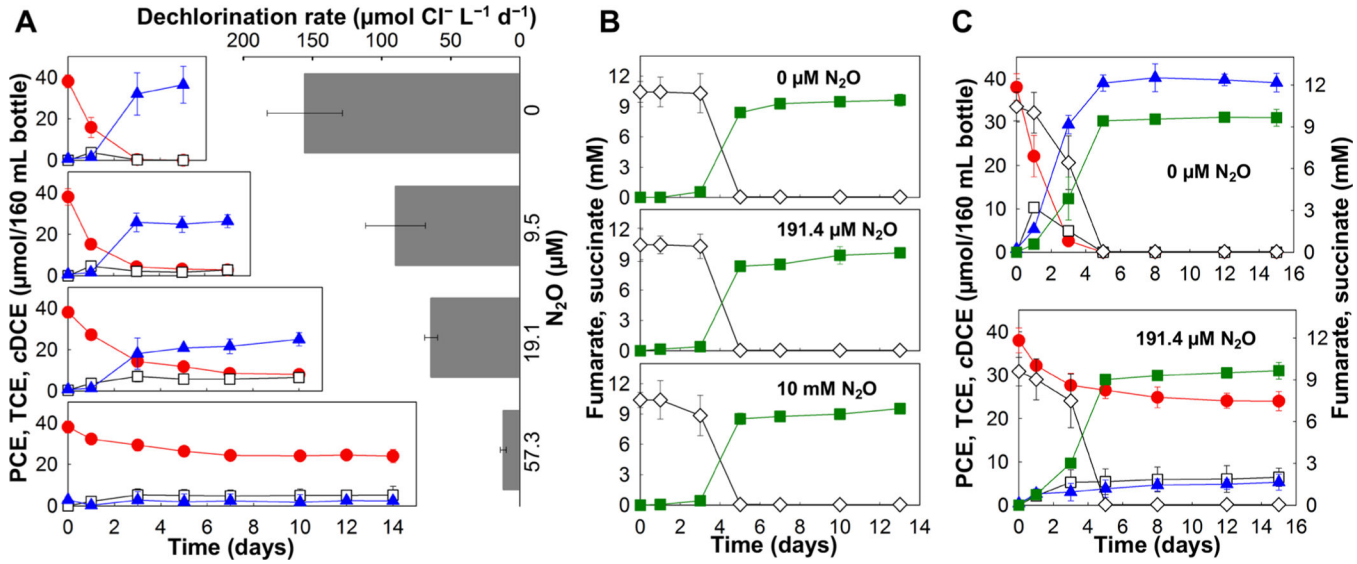

Figure 1.

Effect of N_2O on the consumption of PCE (A), fumarate (B), or both PCE and fumarate (C) as electron acceptors in cultures of the corrinoid−prototrophic bacterium *Geo* strain SZ. (A) PCE-to-*c*DCE reductive dechlorination rates and extents in *Geo* strain SZ cultures without N_2O (top) and in the presence of 9.5, 19.1, and 57.3 μM N_2O. (B) Fumarate-to-succinate reduction in *Geo* strain SZ cultures without N_2O and in the presence of 191.4 μM and 10 mM N_2O. (C) PCE-to-*c*DCE reductive dechlorination and fumarate-to-succinate reduction in *Geo* strain SZ cultures in the absence of N_2O (top) and in the presence of 191.4 μM N_2O (bottom). Solid red circles, PCE; open squares, TCE; solid blue triangles, *c*DCE; open diamonds, fumarate; solid green squares, succinate. Error bars represent the standard deviation (sd) of triplicate cultures.

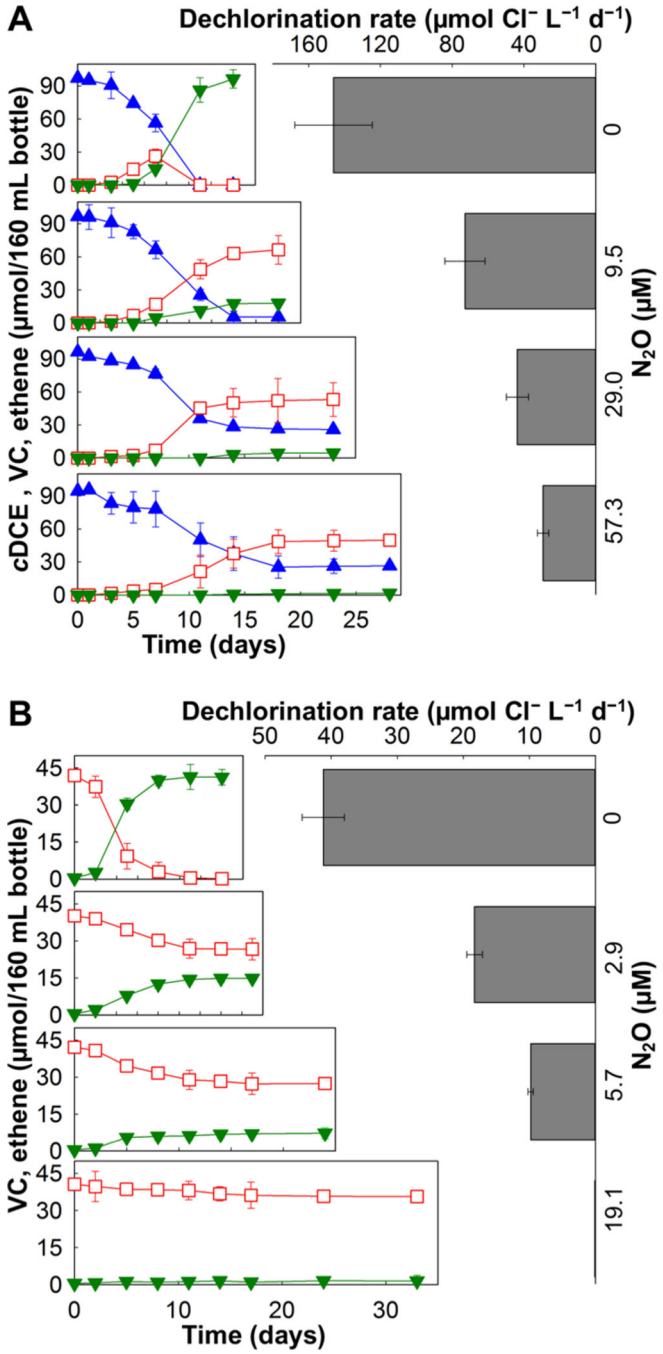

Figure 2.

Effect of N_2O on reductive dechlorination of *c*DCE (A) and VC (B) in corrinoid auxotrophic Dhc strain BAV1. (A) *c*DCE reductive dechlorination rates and extents in *Dhc* strain BAV1 without N_2O (top panel) and in the presence of 9.5, 29.0, and 57.3 μM N_2O. (B) VC reductive dechlorination rates and extents in Dhc strain BAV1 without N_2O (top) and in the presence of 2.9, 5.7, and 19.1 μM N_2O. Solid blue triangles, *c*DCE; open red squares, VC; inverted, solid green triangles, ethene. Error bars represent the sd of triplicate cultures.

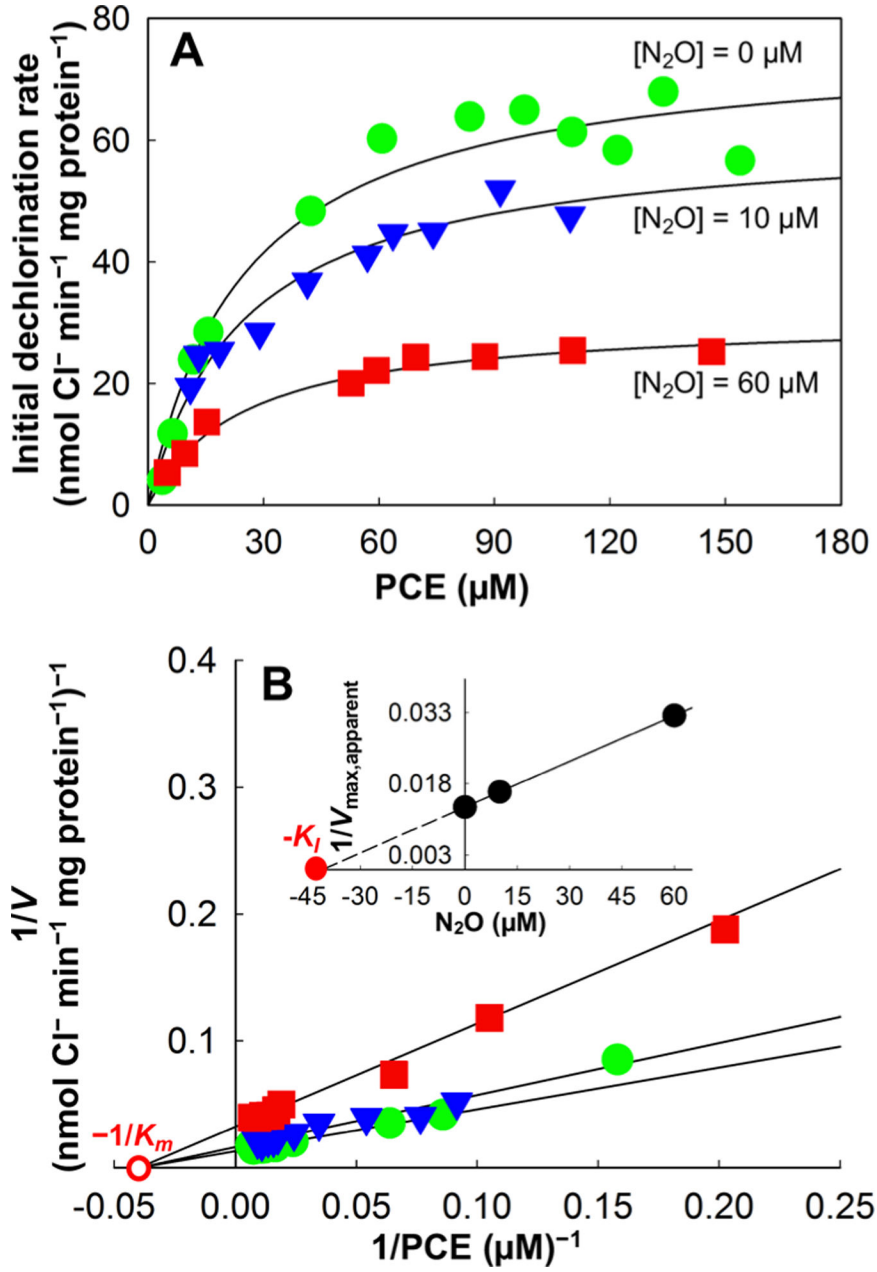

Figure 3.

Kinetics of PCE-to-*c*DCE reductive dechlorination in cell suspensions of *Geo* strain SZ in the presence of increasing concentrations of N_2O. (A) Michaelis−Menten plot of initial PCE-to-*c*DCE dechlorination rates versus PCE concentrations without and in the presence of 10 and 60 μM N_2O. (B) Lineweaver−Burk plot with inserted Dixon plot illustrating N_2O inhibition on PCE-to-*c*DCE reductive dechlorination. Solid lines represent the best fit to each data set based on nonlinear regression using the noncompetitive inhibition model. Solid green circles represent rate data measured in the absence of N_2O, solid blue triangles show rate data measured in the presence of 10 μM N_2O, and solid red squares show rate data

measured in the presence of 60 μM N_2O. Solid and open red circles depict the graphical determination of $-K_I$ and $-1/K_m$, respectively.

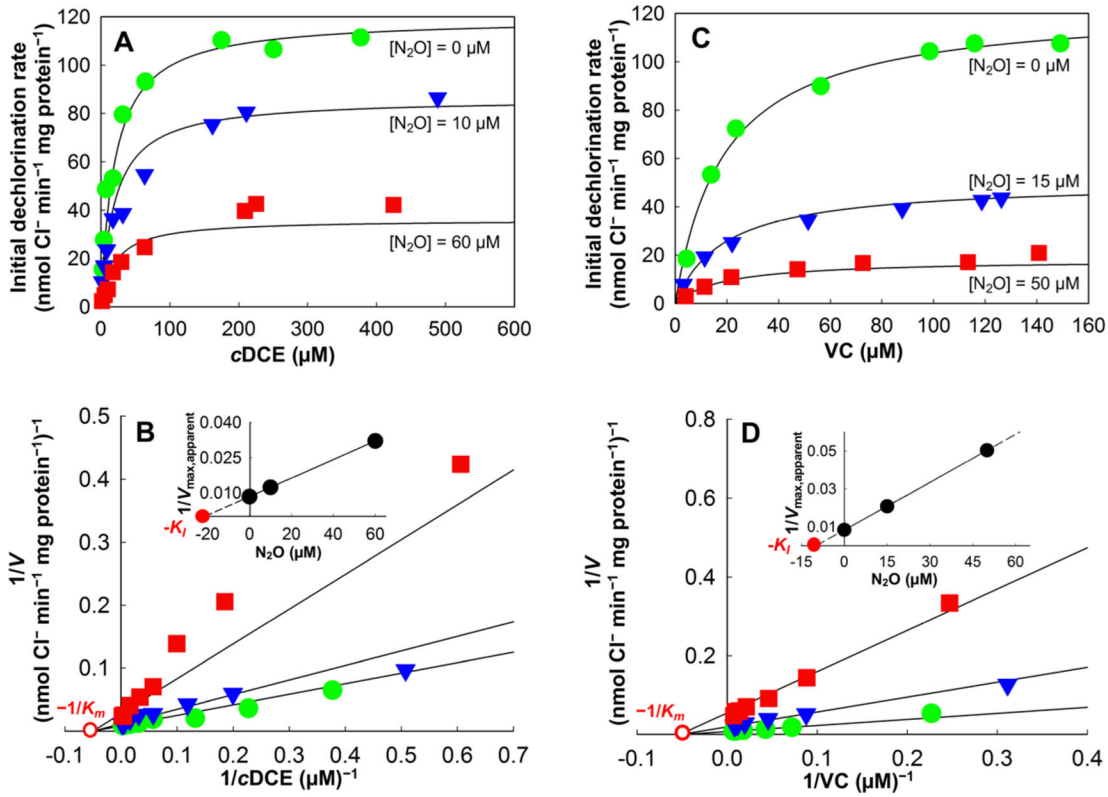

Figure 4.

Kinetics of *c*DCE-to-VC and VC-to-ethene reductive dechlorination in cell suspensions of *Dhc* strain BAV1 in the presence of increasing concentrations of N_2O. (A) Michaelis−Menten plot of initial *c*DCE-to-VC dechlorination in cell suspensions of *Dhc* strain BAV1 without and in the presence of 10 and 60 μM N_2O. (B) Lineweaver−Burk plot with inserted Dixon plot illustrating N_2O inhibition of *c*DCE-to-VC reductive dechlorination. (C) Michaelis−Menten plot of initial VC-to-ethene dechlorination in cell suspensions of *Dhc* strain BAV1 without and in the presence of 15 and 50 μM N_2O. (D) Lineweaver−Burk plot with inserted Dixon plot illustrating N_2O inhibition of VC-to-ethene reductive dechlorination. Solid lines represent the best fit to each data set based on nonlinear regression using the noncompetitive inhibition model. Solid green circles represent rate data measured in the absence of N_2O; solid blue triangles and solid red squares show dechlorination rate data measured in the presence of N_2O (panels A and B, *c*DCE; panels C and D, VC). Solid and open red circles shown in B and D depict the graphical determination of $-K_I$ and $-1/K_m$, respectively.

Table 1.

Kinetic (V_{max}, K_m) and Inhibition (K_I) Parameters for PCE, *c*DCE, and VC Reductive Dechlorination in Cell Suspensions of *Geo* Strain SZ and *Dhc* Strain BAV1 in Response to Increasing N_2O Concentrations[a]

e⁻ acceptor	culture	N_2O (μM)	V_{max} (nmol Cl^- min^{-1} mg $protein^{-1}$)	K_m (μM)	K_I (μM)
PCE	strain SZ	0	76.3 (±2.6)	25.1 (±2.9)	40.8 (±3.8)
		10	61.3 (±4.1)		
		60	30.9 (±4.2)		
*c*DCE	strain BAV1	0	119.4 (±4.1)	19.9 (±2.5)	21.2 (±3.5)
		10	81.1 (±5.1)		
		60	31.2 (±2.4)		
VC	strain BAV1	0	123.3 (±3.2)	18.9 (±1.3)	9.6 (±0.4)
		15	78.9 (±2.1)		
		50	19.9 (±1.3)		

[a]The best fit data were achieved with the Michaelis−Menten noncompetitive inhibition model. Error values represent 95% confidence intervals.